Journal of Materials Chemistry C

PAPER

View Article Online
View Journal | View Issue

Cite this: J. Mater. Chem. C, 2016, 4, 9460

Dicyanovinyl-substituted indolo[3,2-*b*]indole derivatives: low-band-gap π-conjugated molecules for a single-component ambipolar organic field-effect transistor†

Illhun Cho,[a] Sang Kyu Park,[a] Boseok Kang,[b] Jong Won Chung,[a] Jin Hong Kim,[a] Won Sik Yoon,[a] Kilwon Cho[b] and Soo Young Park*[a]

Received 4th July 2016,
Accepted 13th September 2016

DOI: 10.1039/c6tc02777f

www.rsc.org/MaterialsC

A series of low-band-gap π-conjugated molecules comprising *N*,*N*′-dihexylindolo[3,2-*b*]indole as an electron donor (D) and dicyanovinyl as an electron acceptor (A) with A–π–D–π–A architecture have been designed and synthesized to fabricate a single-component ambipolar organic field-effect transistor (OFET). Molecules with different π-bridging units (none, thiophene, and bithiophene) were synthesized and characterized to investigate their structure–property correlation. *Via* the cooperative effects of intramolecular charge transfer (ICT) interactions and extension of conjugation, the band gap of the newly synthesized molecules was reduced to 1.41 eV in the solution state. Among other compounds, **2H2TIDID-DCV** (with a thiophene π-spacer) exhibited highly balanced ambipolar charge transport with hole and electron mobilities of 0.08 $cm^2\ V^{-1}\ s^{-1}$ and 0.09 $cm^2\ V^{-1}\ s^{-1}$, respectively, from a vacuum-deposited OFET device. Spin-coated OFET devices using **OD2TIDID-DCV**, in which the hexyl side chains of **2H2TIDID-DCV** are replaced by 2-octyldodecyl groups, also exhibited an ambipolar charge-transporting nature (mobilities of 9.67×10^{-2} $cm^2\ V^{-1}\ s^{-1}$ for holes and 3.43×10^{-3} $cm^2\ V^{-1}\ s^{-1}$ for electrons). Both **2H2TIDID-DCV** and **OD2TIDID-DCV** exhibited favorable thin-film morphology for the formation of charge-transporting channels, and structural analyses of these films revealed the same molecular packing characteristics of a three-dimensional lamellar π-stacking structure.

Introduction

Research interest in ambipolar organic field-effect transistors (OFETs) has grown significantly because of their potential application to complementary circuits such as inverters without a complicated multi-step deposition process.[1,2] In particular, single-component ambipolar OFETs that simply comprise a single-layer active channel with symmetric source-drain electrodes have attracted much attention owing to their expediency in the practical fabrication of devices.[2–4] In theory, many organic semiconductors are known to transport both types of charge carrier in their solid state if and only if the charge carriers are efficiently injected.[2,5] However, the majority of reported organic semiconductors exhibited unipolar characteristics, *i.e.*, either holes or electrons were transported only, depending on the work function of the electrodes, which was mainly due to the restriction of a high injection barrier for one of the carriers.[6–8] Therefore, among various crucial issues in fabricating single-component ambipolar OFETs, a balanced alignment of the energy levels of the highest occupied molecular orbital (HOMO) and lowest unoccupied molecular orbital (LUMO) of the organic semiconductor relative to the work function of the symmetric electrode is essential for favorable bipolar injection.[2,8–11] In this regard, a wide range of low-band-gap organic materials has been extensively investigated and some π-conjugated structures such as TIPS-pentacenes,[12–14] diketopyrrolopyrroles,[15–18] indigos,[19] isoindigos,[20] and quinoidal oligothiophenes[21–23] have been reported as promising backbone structures for designing high-performance ambipolar semiconductors *via* appropriate engineering of the molecular structure.[24] In spite of extensive materials research into ambipolar OSCs, the effect of molecular structure on the operating mechanism of ambipolar OFETs has seldom been studied. In this regard, the investigation of structure–property correlations based on comprehensive photophysical, electrochemical, and quantum chemical calculation studies is essential for developing high-performance organic semiconductors.

[a] Center for Supramolecular Optoelectronic Materials, Department of Materials Science and Engineering, Seoul National University, 1 Gwanak-ro, Gwanak-gu, Seoul 151-744, Korea. E-mail: parksy@snu.ac.kr
[b] Department of Chemical Engineering, Pohang University of Science and Technology (POSTECH), Pohang 790-784, Korea

† Electronic supplementary information (ESI) available: Additional synthetic procedures, AFM images, and OFET device data. See DOI: 10.1039/c6tc02777f

Very recently, we have synthesized indolo[3,2-*b*]indole (IDID) derivatives as promising p-type organic semiconductors with a remarkable hole mobility of 0.97 $cm^2 V^{-1} s^{-1}$ and versatile processability.[25] Besides the apparent advantages of a pyrrole-fused structure such as facile control of solubility and structural derivatization, the IDID core is characterized by a stronger electron-donating nature than those of other reported pyrrole-fused heteroarene cores (*e.g.*, carbazole and indolocarbazole) owing to the larger proportion of five-membered pyrrole units in the backbone. To examine the possible bipolar injection and transport of carriers, we here designed and synthesized intramolecular charge transfer (ICT)-type IDID derivatives (IDID-DCV derivatives), namely, **2HIDID-DCV**, **2H2TIDID-DCV**, and **2H4TIDID-DCV**, which comprise IDID as an electron donor (D) and dicyanovinyl (DCV) as an electron acceptor (A) with A–π–D–π–A-type architecture. Three different π-linking units (none, thiophene, and bithiophene) were incorporated to study different degrees of ICT interaction and π-conjugation, which enabled both a molecular structure–property correlation and the precise control of electronic characteristics. For an elaborate in-depth analysis of structure–property correlations we also prepared p-type reference molecules, namely, **2HIDID**, **2H2TIDID**, and **2H4TIDID**, on which comprehensive studies were conducted in terms of their theoretical, photophysical, electrochemical, morphological, electrical, and structural characteristics. Among other compounds, **2H2TIDID-DCV** (with a thiophene π-linker) exhibited a dramatically reduced energy band gap (1.62 eV in the solution state), as well as excellent film morphology, which afforded highly balanced ambipolar charge transport with hole and electron mobilities of 0.08 $cm^2 V^{-1} s^{-1}$ and 0.09 $cm^2 V^{-1} s^{-1}$, respectively, in vacuum-deposited (VD) OFET devices. With the aim of fabricating a solution-processable IDID-DCV derivative, **OD2TIDID-DCV** was also synthesized, in which the hexyl side chains of **2H2TIDID-DCV** were replaced by 2-octyldodecyl groups. A spin-coated OFET device using **OD2TIDID-DCV** also exhibited ambipolar charge transport behavior (mobilities of 9.67×10^{-2} $cm^2 V^{-1} s^{-1}$ for holes and 3.43×10^{-3} $cm^2 V^{-1} s^{-1}$ for electrons). To the best of our knowledge, this is the first report of a single-component ambipolar OFET based on a pyrrole-fused heteroacene family, even including the widely studied indolocarbazole derivatives.

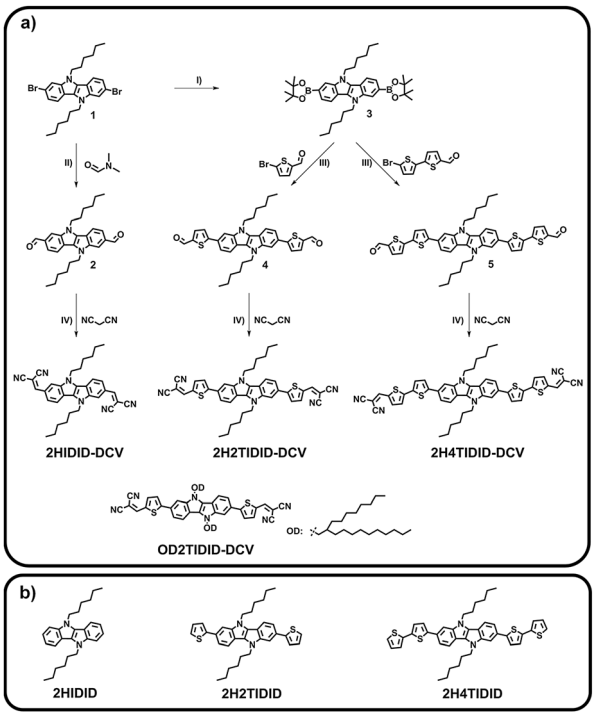

Scheme 1 (a) Synthetic routes to IDID-DCV derivatives and their chemical structures: (I) bis(pinacolato)diborane, $Pd_2(dppf)_2$, KOAc, anhydrous dimethylformamide, (II) *n*-BuLi, tetrahydrofuran, (III) $Pd(PPh_3)_4$, 2 N K_2CO_3, tetrahydrofuran, (IV) Al_2O_3, methylene chloride; (b) chemical structure of IDID reference derivatives.

Result and discussion

To understand the effects of ICT interactions and alterations in the molecular structure on the electronic characteristics of IDID derivatives, and also to fabricate an ambipolar OSC for practical applications, we rationally designed a molecular structure as follows. Using the DCV unit as a strong electron acceptor, we constructed an A–π–D–π–A-type molecular architecture not only to exhibit strong ICT interactions but also to enable efficient electron injection by lowering the LUMO energy level,[26,27] for which purpose the electronic and intramolecular interaction characteristics were delicately tuned by altering the π-linker (none, thiophene, or bithiophene). Based on this idea, we designed a series of three IDID-DCV derivatives, namely, **2HIDID-DCV**, **2H2TIDID-DCV**, and **2H4TIDID-DCV** (Scheme 1). The synthesis of 2,7-dibromo-*N*,*N*′-dihexyl-IDID (compound **1**) was performed according to our previous report,[25] from which IDID-DCV derivatives were successfully synthesized *via* lithium-exchange formylation, palladium-catalyzed borylation, Suzuki–Miyaura cross-coupling, and the Knoevenagel condensation reaction. All three target compounds were carefully characterized by ^1H NMR, ^{13}C NMR, elemental analysis, and mass analysis. The detailed synthetic procedures are described in Scheme 1 and the Experimental section.

For a comprehensive understanding of the newly synthesized IDID-DCV derivatives in terms of their photophysical properties, we also prepared three IDID reference materials, namely, **2HIDID**, **2H2TIDID**, and **2H4TIDID**, which have exactly the same molecular structures as those of **2HIDID-DCV**, **2H2TIDID-DCV**, and **2H4TIDID-DCV**, respectively, but without the acceptor unit (DCV) (see Scheme 1. **2H2TIDID** and **2H4TIDID** were reported earlier,[25] but **2HIDID** was newly synthesized in this work. The detailed synthetic procedure and characterization of **2HIDID** are described in the ESI†).

The electronic characteristics of the IDID-DCV derivatives were determined *via* molecular orbital calculations, UV-vis spectroscopy, and cyclic voltammetry (CV) measurements. The ground-state optimized geometries and electronic structures of the IDID derivatives were calculated within the density functional theory (DFT) by the B3LYP method using the Gaussian 09

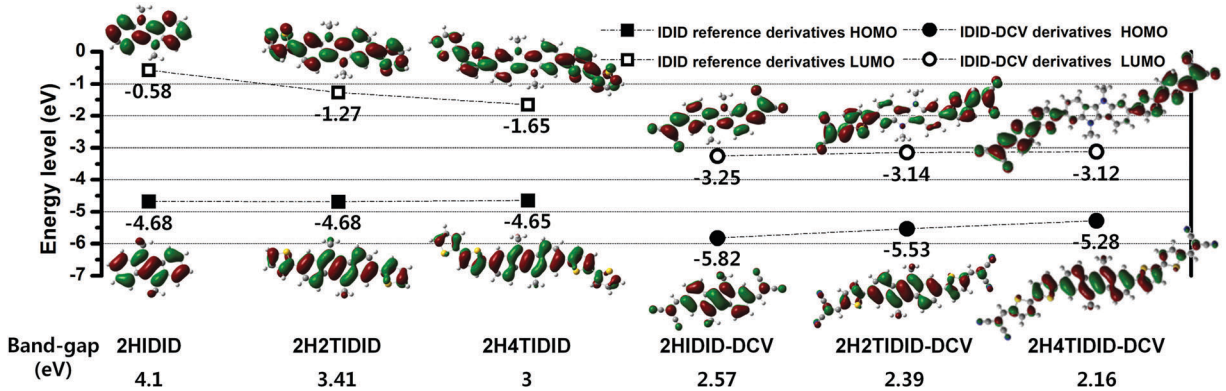

Fig. 1 Plot of calculated energy levels for IDID-DCV derivatives and IDID reference derivatives and their molecular orbital contours (DFT/B3LYP/6-31G(d,p): the alkyl chains were replaced by methyl groups in the calculations).

package with the 6-31G(d,p) basis set. According to the calculated energies of the frontier orbitals shown in Fig. 1, it is noted that the effect of different π-linking units (none, thiophene, or bithiophene) in the IDID-DCV derivatives is quite different from that in the p-type IDID reference derivatives. Because the IDID unit intrinsically has a very low ionization potential, the extension of π-conjugation with thiophene units mostly resulted in stabilization of the LUMO energies with no variation in the HOMO in the case of the p-type reference derivatives. Although both the HOMO and LUMO energies of a given IDID-DCV derivative were strongly stabilized in comparison with those of the respective IDID reference derivative, the actual degree of stabilization increased in the order of the different π-linking units (none > thiophene > bithiophene), as seen in Fig. 1. This can be rationally correlated with the increasing strength of ICT characteristics with a decrease in the D–A distance.

For the empirical study of electronic transitions, the UV-vis absorption spectra of the IDID derivatives were recorded at a concentration of 1×10^{-5} M in solution in tetrahydrofuran (THF) and also for spin-coated films (see Fig. 2; the detailed data are listed in Table 1). In the solution state, all the IDID-DCV derivatives exhibited broad absorption bands consisting of three absorption maxima. Interestingly, the locations of the maxima for the lowest-energy transition corresponding to the ICT transition were virtually the same for all of them (544 nm for **2HIDID-DCV** and 555 nm for **2H2TIDID-DCV** and **2H4TIDID-DCV**), in spite of the lengths of the π-linker being different from each other. This feature can be understood by comparing their absorption spectra with those of the reference derivatives. As shown in Fig. 2c, the IDID-DCV derivatives exhibited different degrees of bathochromic shift in their absorption spectra ($\Delta\lambda_{max}$s, see Table 1), which increased with a decrease in the D–A distance. The fact that the ICT absorption wavelengths among the IDID-DCV derivatives were apparently similar can thus be rationalized on the basis of a reduction in the strength of ICT and the effects of conjugation length. The strength of ICT interactions between IDID and DCV became less for molecules with a larger number of thiophene π-spacers, which at the same time was compensated for by an increase in the length of π-conjugation to give a comparable absorption maximum wavelength. For solid-state samples of the

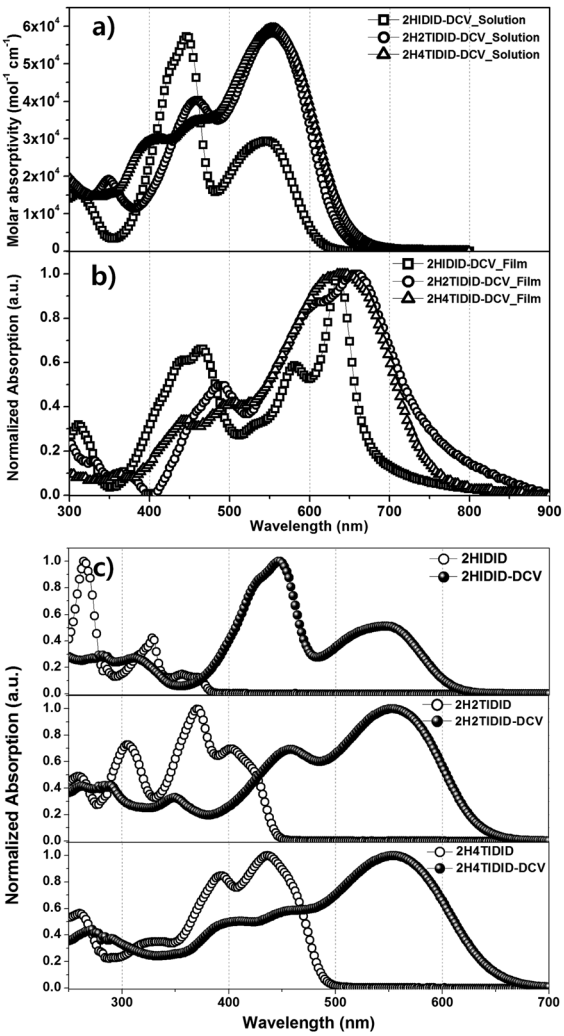

Fig. 2 Absorption spectra of IDID-DCV derivatives in the solution state (a) and film state (b) and each solution-state absorption spectrum with that of the corresponding reference derivative (c).

IDID-DCV derivatives, further bathochromic shifts of 90–100 nm with distinct vibronic features were observed, as shown in Fig. 2b and summarized in Table 1.

Table 1 Optical and electrochemical properties of IDID-DCV derivatives

Compound	Abs. λ_{max}[a] [sol./film/$\triangle\lambda_{max}$, nm]	$\triangle\lambda_{max}$s [nm][b]	HOMO[c] [sol./film, eV]	LUMO[c] [sol./film, eV]	Band gap[d] [sol./film, eV]
2HIDID-DCV	544/636/89	179	−5.34/−5.42	−3.51/−3.71	1.81/1.71
2H2TIDID-DCV	555/657/103	151	−5.08/−5.09	−3.46/−3.86	1.62/1.23
2H4TIDID-DCV	555/641/89	118	−4.90/−4.99	−3.49/−3.74	1.41/1.25

[a] λ_{max} is derived from the maximum for the lowest spin-allowed transition. $\triangle\lambda_{max}$ represents the difference in λ_{max} between the solution state and film state. The absorption spectra of solutions were recorded in THF (at a concentration of 1×10^{-5} M), and the absorption spectra of films were recorded with a spin-coated sample (1500 rpm/60 s, 0.3 wt% in chloroform). [b] $\triangle\lambda_{max}$s represents the absolute difference in λ_{max} between the IDID-DCV derivative and the corresponding IDID reference in the solution state. [c] HOMO and LUMO energy levels were determined by cyclic voltammetry. Solution samples were prepared at 3×10^{-3} M in THF and film samples were prepared on ITO patterned glass by drop-casting. [d] Band gap = $V_{oxidation} - V_{reduction}$.

To investigate the electrochemical properties of the IDID-DCV derivatives, cyclic voltammetry (CV) measurements were made both in the solution state and the solid (film) state. The energies of the HOMO, LUMO, and electrochemical band gap, which were deduced from the first oxidation onset and the first reduction onset of the CV curves, are listed in Table 1. As shown in Fig. 3, the IDID-DCV derivatives exhibited quasi-reversible multi-stage electrochemical oxidation and reduction behavior in a THF solvent. In agreement with the results of DFT calculations in Fig. 1, the LUMO energies of the IDID-DCV derivatives were strongly stabilized and located at similar levels (around −3.5 eV), as seen in Fig. 3 and Table 1. Moreover, the HOMO energies were gradually destabilized with an increase in the length of the π-spacer, *i.e.*, −5.34, −5.08, and −4.90 eV. In consequence, we could achieve quite small band gaps (*i.e.*, down to 1.41 eV) using the compensated ICT interactions between IDID and DCV. In the case of the film state, the HOMO and LUMO energies of the IDID-DCV derivatives were even further stabilized, with the degree of stabilization for the LUMO energies higher than that for the HOMO energies to give smaller band gap energies. Interestingly, the largest stabilization of the LUMO in the solid state, which gave the smallest band gap energy of 1.23 eV, was observed for **2H2TIDID-DCV** (see Table 1), which confirms that the electronic interaction was strongest and most efficient in the tightly packed solid state, which suggests excellent OFET mobility (see below).

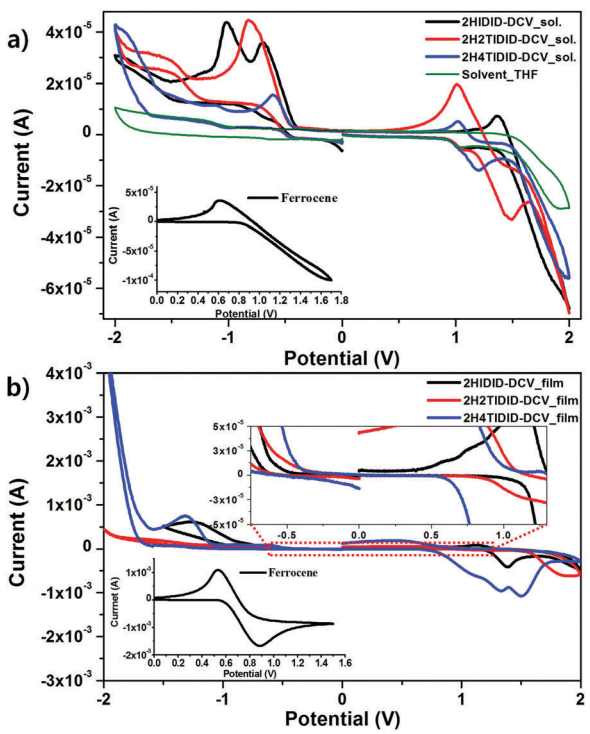

Fig. 3 Cyclic voltammograms of IDID-DCV derivatives in the solution state (a) and film state (b) (insets: ferrocene).

Based on their photophysical and electrochemical properties (*i.e.*, a satisfactorily low band gap with suitable HOMO and LUMO energies in the solid state for efficient bipolar injection from symmetric source-drain electrodes), two of the IDID-DCV derivatives, namely, **2H2TIDID-DCV** and **2H4TIDID-DCV**, were selected for the evaluation of their OFET characteristics. Before the fabrication of the OFET device, however, we examined the surface topography of VD thin films as a function of alterations in the substrate temperature (T_{sub}). As shown in Fig. S1 (ESI†), **2H2TIDID-DCV** films exhibited dense and compact grain features that were suitable for OFET fabrication, whereas **2H4TIDID-DCV** VD films displayed coarse and undefined topological characteristics that were unsuitable for device construction. Therefore, the charge transport characteristics of **2H2TIDID-DCV** were evaluated for ambipolar mobility in the geometry of bottom-gate top-contact (BGTC) VD OFET devices. **2H2TIDID-DCV** was thermally evaporated and deposited on SiO_2/Si substrates treated with octadecyltrichlorosilane (ODTS) at different T_{sub} values from room temperature (RT) to 140 °C to optimize the device performance. As previously reported, OFET devices using 2H2TIDID exhibited typical p-type OFET behavior.[25] In contrast, OFET devices using **2H2TIDID-DCV** displayed ambipolar OFET behaviour, exhibiting typical V-shaped transfer curves and unique output curves with a superlinear regime, as seen in Fig. 4a to f. With an increase in T_{sub}, the hole and electron mobilities increased simultaneously (see Fig. S2 and Table 2, ESI†).

In particular, the electron mobility was much more dramatically increased by altering the deposition temperature (an increase of nearly four orders of magnitude, from 1.5×10^{-5} to 9.2×10^{-2} cm^2 V^{-1} s^{-1}) than was the hole mobility (from 1.8×10^{-3} to 8.2×10^{-2} cm^2 V^{-1} s^{-1}), and the devices that were deposited at a high T_{sub} (>70 °C), exhibited well-balanced hole

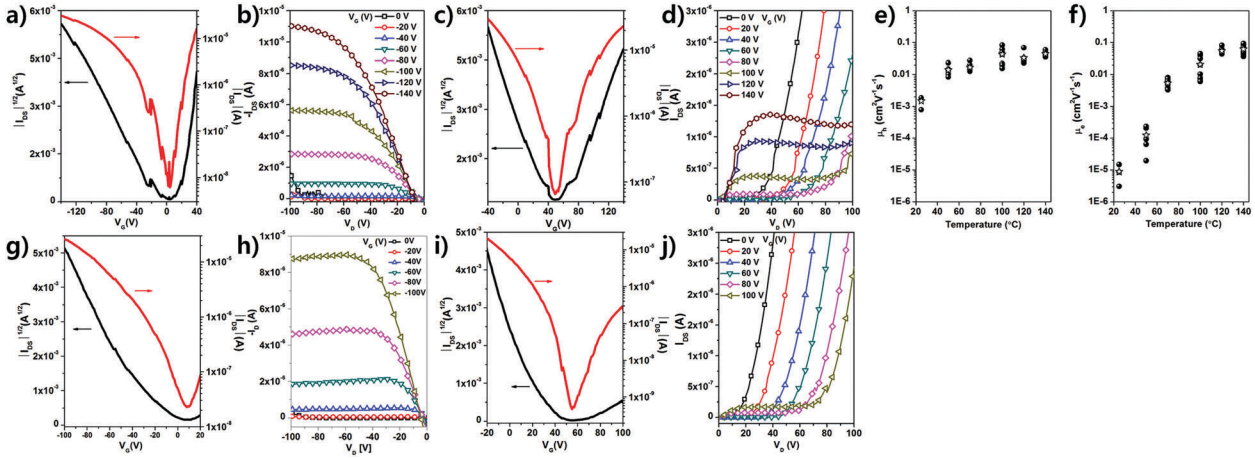

Fig. 4 OFET device characteristics. (a to f) Representative OFET device characteristics of **2H2TIDID-DCV**: (a and c) transfer curves of device formed at a T_{sub} of 120 °C, (b and d) output curves of device formed at a T_{sub} of 120 °C, and (e and f) temperature-dependent mobility for p- and n-channel operation, respectively (the white stars represent average values). (g to j) Characteristics of spin-coated OFET device using **OD2TIDID-DCV** (annealing temperature is 150 °C): (g and i) transfer curves and (h and j) output curves for p- and n-channel operation, respectively.

Table 2 OFET device characteristics

		p-Channel operation			n-Channel operation			
Compound	T_{sub}[a] [°C]	μ_h, max/average[b] [cm^2 V^{-1} s^{-1}]	V_{th} [V][c]	I_{on}/I_{off}	μ_e, max/average[b] [cm^2 V^{-1} s^{-1}]	V_{th}[c] [V]	I_{on}/I_{off}	p/n ratio
2H2TIDID-DCV	RT	$1.85 \times 10^{-3}/1.43 \times 10^{-3}$	−42 (±8)	3×10^4	$1.47 \times 10^{-5}/8.79 \times 10^{-6}$	60 (±5)	2×10^1	125.85
	50	$2.30 \times 10^{-2}/1.39 \times 10^{-2}$	−22 (±12)	1×10^5	$2.32 \times 10^{-4}/1.23 \times 10^{-4}$	100 (±10)	3×10^2	99.14
	70	$2.76 \times 10^{-2}/1.69 \times 10^{-2}$	−9 (±9)	4×10^4	$8.07 \times 10^{-3}/5.39 \times 10^{-3}$	67 (±18)	3×10^3	3.42
	100	$8.28 \times 10^{-2}/4.30 \times 10^{-2}$	−7 (±3)	1×10^3	$4.46 \times 10^{-2}/2.09 \times 10^{-2}$	61 (±10)	5×10^2	1.86
	120	$6.86 \times 10^{-2}/3.30 \times 10^{-2}$	−13 (±4)	4×10^3	$8.13 \times 10^{-2}/5.45 \times 10^{-2}$	61 (±13)	9×10^2	0.84
	140	$5.89 \times 10^{-2}/4.41 \times 10^{-2}$	−15 (±3)	1×10^4	$9.24 \times 10^{-2}/6.21 \times 10^{-2}$	77 (±9)	3×10^3	0.63
2H2TIDID[e]	70	$3.20 \times 10^{-2}/3.00 \times 10^{-2}$	−11 (±2)	1×10^4	—	—	—	—
OD2TIDID-DCV	150[d]	$9.67 \times 10^{-2}/5.28 \times 10^{-2}$	−24 (±9)	4×10^4	$3.42 \times 10^{-3}/1.25 \times 10^{-3}$	50 (±11)	1×10^2	28.27

[a] Substrate temperature in vacuum deposition. [b] The mobilities were derived from the saturation regimes. [c] Average threshold voltages. The values in parentheses represent one standard deviation. [d] Post annealing temperature of spin-coated device (°C). [e] From ref. 25.

and electron mobilities (the ratio of hole mobility to electron mobility was 0.63 at a T_{sub} of 140 °C). Such different tendencies of the variations in electron and hole mobility are most probably due to the sensitivity to trap sites of electron charge carriers being higher than that of hole charge carriers.[28] The increase in mobility could be attributed to the reduced density of trap sites originating from an increase in grain size, as was rationalized from a study of surface topography using atomic force microscopy (AFM) measurements. As shown in Fig. 5a to f, the surface topography of **2H2TIDID-DCV** film was transformed from a uniform film (root-mean-square roughness value of 0.7 nm) into a highly ordered crystalline film with terrace-structured grains with an increase in T_{sub}; structured grains developed from a T_{sub} of 70 °C, and micron-sized grains were observed from a T_{sub} of 120 °C. By correlating charge carrier mobility with surface topography, it was found that the terrace-structured and enlarged grains were responsible for the favorable intermolecular packing structure for the transport of both hole and electron charge carriers (see below).

To demonstrate a solution-processable IDID-DCV derivative, we additionally synthesized **OD2TIDID-DCV**, in which the linear hexyl side chains in **2H2TIDID-DCV** were replaced by branched 2-octyldodecyl groups (see Scheme 1 and Scheme S2; detailed synthetic procedures and characterizations are described in the ESI†). Spin-coated OFET devices using **OD2TIDID-DCV** were fabricated and characterized for the same OFET structure and geometry as the VD devices, but with the semiconducting material (**OD2TIDID-DCV**) deposited by a spin-coating method. As shown in Fig. 4g to j, the optimized spin-coated OFET device (post annealing temperature of 150 °C) exhibited ambipolar charge transport behaviour, with hole and electron mobilities of 9.6×10^{-2} cm^2 V^{-1} s^{-1} and 3.4×10^{-3} cm^2 V^{-1} s^{-1}, respectively. With respect to the values of charge carrier mobility, solution-processed devices using **OD2TIDID-DCV** exhibited slightly higher values of hole mobility but relatively lower values of electron mobility than those of **2H2TIDID-DCV**. Such different values of mobility were due to the somewhat different π–π distances (see below) and rather smaller grain sizes in comparison with those of the optimized VD device (see Fig. 5g).

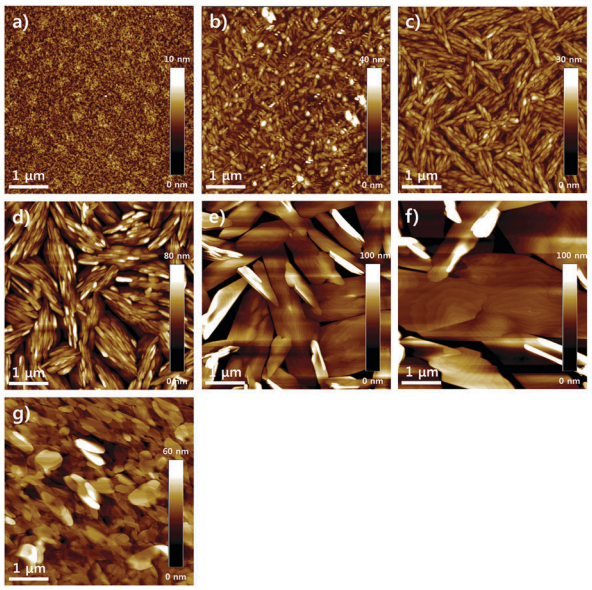

Fig. 5 AFM surface topologies (height images, 5 μm × 5 μm) of **2H2TIDID-DCV** VD thin films formed at different values of T_{sub}: (a) RT; (b) 50 °C; (c) 70 °C; (d) 100 °C; (e) 120 °C; (f) 140 °C, and **OD2TIDID-DCV** spin-coated film (g) annealed at 150 °C.

In any case, the experimentally confirmed ambipolarity in the devices using **2H2TIDID-DCV** and **OD2TIDID-DCV** suggests that 2TIDID-DCV is a promising π-conjugated backbone for single-component ambipolar OFETs.

To investigate the molecular packing structure in the organic semiconductor samples, analyses by out-of-plane X-ray diffraction (XRD), powder XRD, and 2D grazing incidence X-ray diffraction (2D-GIXD) were carried out. Fig. 6a shows the out-of-plane XRD patterns of **2H2TIDID-DCV** thin films. Whereas samples formed at a low T_{sub} (RT and 50 °C) exhibited quite weak diffraction peaks, samples that were deposited at a high T_{sub} (over 70 °C) exhibited sharp and strong diffraction peaks up to the third (300) order at 2 theta values of 8.37°, 16.78°, and 25.28°; this could be interpreted as lamellar diffraction with a *d*-spacing of 10.58 Å. From the powder XRD pattern (Fig. 6b), identical lamellar diffraction peaks to those of out-of-plane XRD could be observed at almost the same 2 theta values (8.36°, 16.67°, and 25.16°) and moreover we could recognize a diffraction peak in the wide-angle region (24.9°), which might be interpreted as corresponding to the π–π distance with a *d*-spacing of 3.57 Å (inset of Fig. 6b). The 2D-GIXD result for a **2H2TIDID-DCV** thin film could further support our interpretation; we observed diffraction peaks corresponding to lamellar and π–π *d*-spacings at values of q_z of 0.60 Å^{-1} (10.47 Å) and q_{xy} of 1.76 Å^{-1} (3.57 Å), respectively. Moreover, the 2D-GIXD patterns of an **OD2TIDID-DCV** spin-coated film also exhibited a similar result to that for **2H2TIDID-DCV**, *i.e.*, semiconductor molecules are oriented in exactly the same manner as that of **2H2TIDID-DCV** VD film but with different values of the *d*-spacing (the values of the lamellar spacing and π–π spacing are 17.9 Å and 3.64 Å, respectively). *Via* a comprehensive correlation between XRD, DFT calculations, and the results of AFM surface topography shown in Fig. 6, we could conclude that **2H2TIDID-DCV** (and **OD2TIDID-DCV**) molecules are oriented on the substrate in an edge-on manner and their π-planes are stacked in a direction parallel to the surface. On the other hand, the van der Waals interactions of *N*-aliphatic chains enable **2H2TIDID-DCV** and **OD2TIDID-DCV** to adopt a well-organized three-dimensional lamellar structure with lamellar spacings of 10.58 Å and 17.9 Å, respectively (see Fig. 6j).

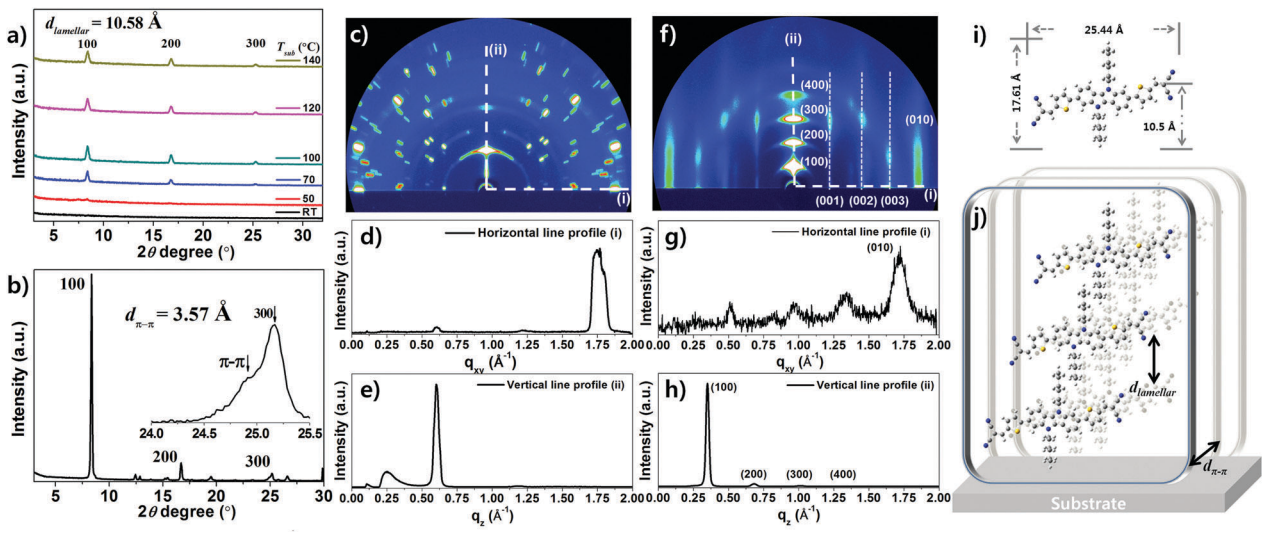

Fig. 6 (a) Out-of-plane XRD patterns of **2H2TIDID-DCV** VD films formed at different values of T_{sub}; (b) powder XRD pattern of **2H2TIDID-DCV** powder; (c) 2D-GIXD diffraction pattern image of **2H2TIDID-DCV** VD film (T_{sub} = 140 °C); (d and e) horizontal and vertical line profiles of (c), respectively; (f) 2D-GIXD diffraction pattern image of **OD2TIDID-DCV** film; (g and h) horizontal and vertical line profiles of (f), respectively; (i) calculated molecular size of **2H2TIDID-DCV**; (j) schematic diagram of packing structure of **2H2TIDID-DCV**.

Conclusions

We have designed and successfully synthesized A–π–D–π–A-type IDID-DCV derivatives with different π-spacers. It was found that compensated ICT interactions between IDID and DCV in 2TIDID-DCV derivatives (with a thiophene π-spacer) and their efficient electronic interactions in a three-dimensional lamellar π-stacking structure gave rise to a dramatically reduced energy band gap, as well as excellent film morphology. As a consequence, a VD OFET device using **2H2TIDID-DCV** exhibited highly balanced ambipolar charge transport with hole and electron mobilities of 0.08 $cm^2\ V^{-1}\ s^{-1}$ and 0.09 $cm^2\ V^{-1}\ s^{-1}$, respectively, and spin-coated OFET devices using **OD2TIDID-DCV** also exhibited ambipolar charge transport behavior (mobilities of $9.67 \times 10^{-2}\ cm^2\ V^{-1}\ s^{-1}$ for holes and $3.43 \times 10^{-3}\ cm^2\ V^{-1}\ s^{-1}$ for electrons).

Experimental section

Synthesis

The final products were synthesized according to the synthetic procedure shown in Scheme 1. 2,7-Dibromo-5,10-dihexyl-5,10-dihydroindolo[3,2-*b*]indole (2,7-dibromo-*N*,*N*′-dihexyl-IDID) was synthesized according to our previous report.[25] Unless stated otherwise, all reagents were purchased from Sigma Aldrich, TCI, and Alfa Aesar.

Synthesis of 5,10-dihexyl-5,10-dihydroindolo[3,2-*b*]indole-2,7-dicarbaldehyde (2). A 100 mL round-bottomed flask equipped with a magnetic stirrer bar was heated under reduced pressure and backfilled with Ar three times. A solution of compound **1** (200 mg, 0.375 mmol) in anhydrous tetrahydrofuran (THF) in the heated reaction vessel was cooled to −17 °C. Afterwards, *n*-butyllithium (*n*-BuLi, 1.6 M solution, 0.36 mL, 0.902 mmol) was added slowly. One hour later, dimethylformamide (DMF, 69 μL, 0.902 mmol) was added to the reaction mixture and then the reaction vessel was warmed to room temperature. After the reaction had finished, the reaction mixture was quenched with distilled water (200 mL) and the organic compounds were extracted with methylene chloride (DCM). The combined organic phase was separated and concentrated. The crude product was purified by column chromatography (ethyl acetate (EA)/*n*-hexane (*n*-hex.); 1 : 19, v/v) to afford compound **2** as a yellow solid (90 mg, 55.3%). ^{1}H NMR (300 MHz, $CDCl_3$, δ): 10.14 (s, 2H), 8.04 (s, 2H), 7.98 (d, J = 8.22 Hz, 2H), 7.74 (d, J = 8.19 Hz, 2H), 4.58 (t, J = 7.14 Hz, 4H), 2.00 (m, J = 7.41 Hz, 4H), 1.44–1.25 (m, 12H), 0.87 (t, J = 7.02 Hz, 6H).

Synthesis of 2HIDID-DCV. A mixed solution of compound **2** (200 mg, 0.462 mmol), malononitrile (67.9 mg, 1.017 mmol), Al_2O_3 (377 mg, 3.698 mmol), and DCM (50 mL) was vigorously stirred for 2 hours at room temperature. After the reaction had finished, the reaction mixture was filtered through a Celite plug to remove residual Al_2O_3 and the filtrate was concentrated under reduced pressure. The crude product was purified by flash column chromatography (THF) and subsequently by recrystallization (EA) to afford **2HIDID-DCV** as a dark purple solid (220 mg, 90.3%). ^{1}H NMR (500 MHz, tetrahydrofuran-d_8, δ): 8.30 (s, 2H), 8.24 (s, 2H), 8.13 (d, J = 8.5 Hz, 2H), 7.86 (d, J = 8.5 Hz, 2H), 4.64 (t, J = 7.5 Hz, 4H), 2.00 (q, J = 7.5 Hz, 4H), 1.43 (q, J = 7.5 Hz, 4H), 1.35–1.24 (m, 8H), 0.83 (t, J = 7.5 Hz, 6H). ^{13}C NMR (500 MHz, tetrahydrofuran-d_8, δ): 161.30, 142.50, 131.37, 127.80, 121.68, 120.41, 117.81, 115.66, 115.08, 115.04, 79.72, 46.40, 32.63, 31.28, 27.77, 23.54, 14.43. HRMS (FAB, *m*/*z*) calcd. for $C_{34}H_{34}N_6$: 526.28; found: 526.2851. Elem. anal. calcd. for $C_{34}H_{34}N_6$: C 77.54, H 6.51, N 15.96; found: C 77.4905, H 6.5662, N 15.8965.

Synthesis of 5,10-dihexyl-2,7-bis(4,4,5,5-tetramethyl-1,3,2-dioxaborolan-2-yl)-5,10-dihydroindolo[3,2-*b*]indole (3). A 100 mL round-bottomed flask equipped with a magnetic stirrer bar and a reflux condenser was heated under reduced pressure and backfilled with Ar three times. Compound **1** (1.00 g, 1.878 mmol), bis(pinacolato)diborane (1.06 g, 4.133 mmol), [1,1′-bis(diphenylphosphino)ferrocene]dichloropalladium(II) (345 mg, 0.413 mmol), potassium acetate (1.10 g, 11.271 mmol), and anhydrous DMF (35 mL) were added and then gently refluxed for 24 hours. After the reaction had finished, the reaction mixture was quenched with brine (300 mL) and extracted with DCM. The combined organic phase was dried with $MgSO_4$ and concentrated under reduced pressure. The crude product was purified by column chromatography (EA/*n*-hex.; 1 : 9, v/v) to afford compound **3** as a yellow solid (350 mg, 41%). ^{1}H NMR (300 MHz, $CDCl_3$, δ): 7.93 (s, 2H), 7.84 (d, J = 7.86 Hz, 2H), 7.62 (d, J = 7.86 Hz, 2H), 4.55 (t, J = 6.93 Hz, 4H), 1.98 (q, J = 6.57 Hz, 4H), 1.39 (s, 24H), 1.29 (m, 12H), 0.86 (t, J = 6.72 Hz, 6H).

Synthesis of 5,5′-(5,10-dihexyl-5,10-dihydroindolo[3,2-*b*]-indole-2,7-diyl)bis(thiophene-2-carbaldehyde) (4). Compound **3** (205 mg, 0.223 mmol), 5-bromothiophene-2-carbaldehyde (131.3 mg, 0.469 mmol), tetrakis(triphenylphosphino)-palladium(0) (37.38 mg, 0.032 mmol), a 2 N aqueous solution of K_2CO_3 (10 mL), and THF (20 mL) were added to a 100 mL round-bottomed flask and the reaction vessel was evacuated and backfilled with Ar. After that, the reaction mixture was gently refluxed for 12 hours. After the reaction had finished, the reaction mixture was quenched with a 1 N aqueous solution of HCl (300 mL) and extracted with DCM. The combined organic phase was dried with $MgSO_4$ and concentrated under reduced pressure. The crude product was purified by flash column chromatography (EA/*n*-hex.; 1 : 2, v/v) and recrystallization (EA) to afford compound **4** as a red solid (190 mg, 94%). ^{1}H NMR (300 MHz, DMSO-d_6, δ): 9.91 (s, 2H), 8.13 (s, 2H), 8.07 (d, J = 4.05 Hz, 2H), 8.00 (d, J = 8.37 Hz, 2H), 7.78 (d, J = 3.96 Hz, 2H), 7.58 (d, J = 8.40 Hz, 2H), 4.68 (t, J = 6.48 Hz, 4H), 1.88 (q, J = 6.57 Hz, 4H), 1.23 (m, 12H), 0.81 (t, J = 6.57 Hz, 6H).

Synthesis of 2H2TIDID-DCV. 2H2TIDID-DCV was synthesized by the same synthetic procedure as that used for **2HIDID-DCV**, using compound **4** (166 mg, 0.279 mmol), malononitrile (40.6 mg, 0.615 mmol), Al_2O_3 (0.228 g, 2.535 mmol), and DCM (50 mL). The crude product was purified by flash column chromatography (THF) and subsequently by recrystallization (EA) to afford **2H2TIDID-DCV** as a dark purple solid (0.189 g, 98%). ^{1}H NMR (500 MHz, tetrahydrofuran-d_8, δ): 8.23 (s, 2H), 8.01 (d, J = 1.5 Hz, 2H), 7.98 (d, J = 8.5 Hz, 2H), 7.86 (d, J = 4 Hz, 2H), 7.73 (d, J = 4 Hz, 2H), 7.61 (dd, J = 8.5 Hz, 1.5 Hz, 2H), 4.66

(t, J = 7 Hz, 4H), 2.00 (q, J = 7.5 Hz, 4H), 1.45 (q, J = 7.5 Hz, 4H), 1.38–1.25 (m, 8H), 0.85 (t, J = 7.5 Hz, 6H). ^{13}C NMR (500 MHz, tetrahydrofuran-d_8, δ): 158.93, 151.96, 142.73, 141.77, 125.19, 119.90, 118.46, 116.19, 115.45, 114.78, 109.18, 45.98, 32.70, 31.35, 27.73, 23.57, 14.46. HRMS (FAB, m/z) calcd. for $C_{42}H_{38}N_6S_2$: 690.26; found: 690.2563. Elem. anal. calcd. for $C_{42}H_{38}N_6S_2$: C 73.01, H 5.54, N 12.16, S 9.28; found: C 73.0165, H 5.5255, N 12.1216, S 9.2924.

Synthesis of 5′,5‴-(5,10-dihexyl-5,10-dihydroindolo[3,2-*b*]-indole-2,7-diyl)bis([2,2′-bithiophene]-5-carbaldehyde) (5). Compound **5** was synthesized by the same synthetic procedure as that used for compound **4**, using compound **3** (170 mg, 0.271 mmol), 5′-bromo-[2,2′-bithiophene]-5-carbaldehyde (135 mg, 0.569 mmol), tetrakis(triphenylphosphino)palladium(0) (32 mg, 0.027 mmol), a 2 N aqueous solution of K_2CO_3 (10 mL), and THF (20 mL). The crude product was purified by column chromatography ($CHCl_3$/EA/n-hex.; 3 : 1 : 6, v/v) and subsequently by recrystallization (EA) to afford compound **5** as a red solid (162 mg, 78%). ^{1}H NMR (300 MHz, tetrahydrofuran-d_8, δ): 9.83 (s, 2H), 7.90 (d, J = 8.28 Hz, 2H), 7.83 (s, 2H), 7.79 (d, J = 3.9 Hz, 2H), 7.48–7.46 (m, 6H), 7.39 (d, J = 3.9 Hz, 2H), 4.61 (t, J = 6.9 Hz, 4H), 1.98 (q, J = 7.47 Hz, 4H), 1.46-1.25 (m, 12H), 0.49 (t, J = 7.08 Hz, 6H).

Synthesis of 2H4TIDID-DCV. 2H4TIDID-DCV was synthesized by the same synthetic procedure as that used for **2HIDID-DCV**, using compound **5** (162 mg, 0.213 mmol), malononitrile (43 mg, 0.640 mmol), Al_2O_3 (0.228 g, 1.921 mmol), and DCM (60 mL). The crude product was purified by flash column chromatography (THF) and subsequently by recrystallization (THF) to afford **2H4TIDID-DCV** as a black solid (0.110 g, 60%). ^{1}H NMR (500 MHz, tetrahydrofuran-d_8, δ): 8.14 (s, 2H), 7.90 (d, J = 8.5 Hz, 2H), 7.84 (s, 2H), 7.78 (d, J = 4 Hz, 2H), 7.56 (d, J = 3.5 Hz, 2H), 7.49 (m, 4H), 7.44 (d, J = 4 Hz, 2H), 4.61 (t, J = 7 Hz, 4H), 2.03 (m, 4H), 1.48 (q, J = 7 Hz, 4H), 1.39-1.27 (m, 8H), 0.85 (t, J = 7 Hz, 6H). HRMS (FAB, m/z) calcd. for $C_{50}H_{42}N_6S_4$: 854.24; found: 854.2363. Elem. anal. calcd. for $C_{50}H_{42}N_6S_4$: C 70.23, H 4.95, N 9.83, S 15.0; found: C 69.8566, H 5.0406, N 9.8086, S 15.0143. (We could not obtain ^{13}C NMR data owing to the insufficient solubility of **2H4TIDID-DCV** in common NMR solvents such as $CDCl_3$ or tetrahydrofuran-d_8.)

Characterization

The chemical structures of the newly synthesized materials were fully identified by ^{1}H NMR, ^{13}C NMR (Bruker Advance 300 and Advance 500), GC-MS (JEOL, JMS-700) and elemental analysis (CE Instruments EA1110). UV-vis spectra were recorded on a Shimadzu UV-1650PC. The HOMO and LUMO energy levels of the organic materials were determined from cyclic voltammetry (CV) measurements. CV measurements were performed using a 273A (Princeton Applied Research) with a one-compartment platinum working electrode, a platinum wire counter electrode, and a quasi-Ag^+/Ag electrode as a reference electrode. The measurements were performed in a 0.5 mM solution in tetrahydrofuran with 0.1 M tetrabutylammonium tetrafluoroborate (TBATFB) as a supporting electrolyte and acetonitrile with 0.1 M TBATFB for the films as a supporting electrolyte at a scan rate of 50 mV s^{-1}. Each oxidation and reduction potential was calibrated using ferrocene as a reference. The film surface topologies were determined with a Bruker Nanoscope III Multimode SPM in tapping mode using a RTESP cantilever. Out-of-plane X-ray diffraction and powder X-ray diffraction measurements were performed using a Bruker D8 Advance X-ray diffractometer. Two-dimensional grazing incidence X-ray diffraction measurements were performed at the 3C beamline of Pohang Acceleration Laboratory. Density functional theory (DFT) calculations were performed by the B3LYP method using the Gaussian 09 package with the 6-31G(d,p) basis set. The I–V characteristics of all devices were measured using a Keithley 4200 SCS analyzer.

OFET device fabrication and measurement

To prepare the substrates, SiO_2/Si substrates (p-doped, 300 nm) were rinsed with acetone and isopropyl alcohol sequentially for 10 minutes in an ultrasonicator, followed by treatment for 15 minutes with UV (360 nm) and O_3. For the fabrication of thermally evaporated vacuum-deposited OFET devices, octadecyltrichlorosilane (ODTS) was treated as a self-assembled monolayer (SAM) on the prepared substrate to reduce the number of charge trap sites as well as to enlarge domains. ODTS was treated in the vapor phase in a vacuum oven and then the substrates were passed into a nitrogen-filled glove box. Organic semiconductor active layers with a thickness of 30 nm were thermally deposited at a deposition rate of 0.1–0.2 Å s^{-1} and different substrate temperatures (T_{sub}: room temperature, 50, 70, 100, 120, and 140 °C) under a vacuum of 7×10^{-7} Torr. As the source and drain electrodes, gold (Au) with a thickness of 50 nm was thermally deposited at a deposition rate of 0.2–0.3 Å s^{-1}. For the fabrication of spin-coated OFET devices, the same procedure for substrate preparation was performed as with the VD devices. **OD2TIDID-DCV** was dissolved in chloroform (0.3–0.4 weight%) and spin-coated at 1500–3000 rpm for 1 minute in a nitrogen-filled glove box and then the substrates were annealed at different temperatures from room temperature to 150 °C. The source and drain electrodes were thermally deposited under the same conditions as were used for the fabrication of VD devices. The I–V characteristics of all the OFETs were measured in a nitrogen-filled glove box using a Keithley 4200 SCS instrument connected to a probe station. All the OFET characteristics were determined from the transfer curve in the saturation regime. For the calculations of charge carrier mobility, we measured the channel width and length of the individual devices using an optical microscope.

Acknowledgements

This research was supported by the National Research Foundation of Korea (NRF) through a grant funded by the Korean government (MSIP; No. 2009-0081571[RIAM0417-20150013]).

References

1 J. G. Champlain, *Appl. Phys. Lett.*, 2011, **99**, 123502.
2 J. Zaumseil and H. Sirringhaus, *Chem. Rev.*, 2007, **107**, 1296.
3 S.-I. Noro, T. Takenobu, Y. Iwasa, H.-C. Chang, S. Kitagawa, T. Akutagawa and T. Nakamura, *Adv. Mater.*, 2008, **20**, 3399.
4 T. D. Anthopoulos, S. Setayesh, E. Smits, M. Cölle, E. Cantatore, B. Bore, P. W. M. Blom and D. M. Leeuw, *Adv. Mater.*, 2006, **18**, 1900.
5 K. Liu, C.-L. Song, Y.-C. Zhou, X.-Y. Zhou, X.-J. Pan, L.-Y. Cao, C. Zhang, Y. Liu, X. Gong and H.-L. Zhang, *J. Mater. Chem. C*, 2015, **3**, 4188.
6 J. Bardeen, *Phys. Rev.*, 1947, **71**, 717.
7 T. Kanagasekaran, H. Shimotani, S. Ikeda, H. Shang, R. Kumashiro and K. Tanigake, *Appl. Phys. Lett.*, 2015, **107**, 043304.
8 E. J. Meijer, D. M. D. Leeuw, S. Setayesh, E. V. Veenendaal, B.-H. Huisman, P. W. M. Blom, J. C. Hummelen, U. Scherf and T. M. Klapwijk, *Nat. Mater.*, 2003, **2**, 678.
9 B. Jaeckel, J. B. Sambur and B. A. Parkinson, *Appl. Phys. Lett.*, 2008, **103**, 063719.
10 T. Yasuda, T. Goto, K. Fujita. and T. Tsutsui, *Appl. Phys. Lett.*, 2004, **85**, 2098.
11 J.-Y. Hu, M. Nakano, I. Osaka and K. Takimiya, *J. Mater. Chem. C*, 2015, **3**, 4244.
12 M. L. Tang, A. D. Reichardt, N. Miyaki, R. M. Stoltenberg and Z. Bao, *J. Am. Chem. Soc.*, 2008, **130**, 6064.
13 Y.-Y. Liu, C.-L. Song, W.-J. Zeng, K.-G. Zhou, Z.-F. Shi, C.-B. Ma, F. Yang, H.-L. Zhang and X. Gong, *J. Am. Chem. Soc.*, 2010, **132**, 16349.
14 C.-L. Song, C.-B. Ma, F. Yang, W.-J. Zeng, H.-L. Zhang and X. Gong, *Org. Lett.*, 2011, **13**, 2880.
15 J. Lee, A.-R. Han, H. Yu, T. J. Shin, C. Yang and J. H. Oh, *J. Am. Chem. Soc.*, 2013, **135**, 9540.
16 B. Sun, W. Hong, Z. Yan, H. Aziz and Y. Li, *Adv. Mater.*, 2014, **26**, 2636.
17 L. Wang, X. Zhang, H. Tian, Y. Lu, Y. Geng and F. Wang, *Chem. Commun.*, 2013, **49**, 11272.
18 A. Riaño, P. M. Burrezo, M. J. Mancheño, A. Timalsina, J. Smith, A. Facchetti, T. J. Marks, H. T. L. Navarrete, J. L. Segura, J. Casado and R. P. Ortiz, *J. Mater. Chem. C*, 2014, **2**, 6376.
19 M. Irimia-Vladu, E. D. Głowacki, P. A. Troshin, G. Schwabegger, L. Leonat, D. K. Susarova, O. Krystal, M. Ullah, Y. Kanbur, M. A. Bodea, V. F. Razumov, H. Sitter, S. Bauer and N. S. Sariciftci, *Adv. Mater.*, 2012, **24**, 375.
20 I. Meager, M. Nikolka, B. C. Schroeder, C. B. Nielsen, M. Planells, H. Bronstein, J. W. Rumer, D. I. James, R. S. Ashraf, A. Sadhanala, P. Hayoz, J.-C. Flores, H. Sirringhaus and I. McCulloch, *Adv. Funct. Mater.*, 2014, **24**, 7109.
21 J. C. Ribierre, L. Zhao, S. Furukawa, T. Kikitsu, D. Inoue, A. Muranaka, K. Takaishi, T. Muto, S. Matsumoto, D. Hashizume, M. Uchiyama, P. André, C. Adachi and T. Aoyama, *Chem. Commun.*, 2015, **51**, 5836.
22 J. Li, X. Qiao, Y. Xiong, H. Li and D. Zhu, *Chem. Mater.*, 2014, **26**, 5782.
23 J. C. Ribierre, S. Watanabe, M. Matsumoto, T. Muto, D. Hashizume and T. Aoyama, *J. Phys. Chem. C*, 2011, **115**, 20703.
24 K. Zhou, H. Dong, H.-L. Zhang and W. Hu, *Phys. Chem. Chem. Phys.*, 2014, **16**, 22448.
25 I. Cho, S. K. Park, B. Kang, J. W. Chung, J. H. Kim, K. Cho and S. Y. Park, *Adv. Funct. Mater.*, 2016, **26**, 2966.
26 T. Qi, Y. Liu, W. Qiu, H. Zhang, X. Gao, Y. Liu, K. Lu, C. Du, G. Yu and D. Zhu, *J. Mater. Chem.*, 2008, **18**, 1131.
27 X. Lu, S. Fan, J. Wu, X. Jia, Z.-S. Wang and G. Zhou, *J. Org. Chem.*, 2014, **79**, 6480.
28 H. Dong, X. Fu, J. Liu, Z. Wang and W. Hu, *Adv. Mater.*, 2013, **25**, 6158.

